Quantifying ecological thresholds from response surfaces

Heather E. Lintz [a,*], Bruce McCune [a], Andrew N. Gray [b], Katherine A. McCulloh [c]

[a] Department of Botany and Plant Pathology, Oregon State University, Corvallis, OR, United States
[b] USDA Forest Service, PNW Research Station, Corvallis, OR, United States
[c] Department of Wood Science and Engineering, Oregon State University, Corvallis, OR, United States

ARTICLE INFO

ABSTRACT

Ecological thresholds are abrupt changes of ecological state. While an ecological threshold is a widely accepted concept, most empirical methods detect them in time or across geographic space. Although useful, these approaches do not quantify the direct drivers of threshold response. Causal understanding of thresholds detected empirically requires their investigation in a multi-factor domain containing the direct drivers (often referred to as state space). Here, we present an approach to quantify thresholds from response surfaces modeled empirically in state space. We present two indices of shape attributes measured from response surfaces. The response surfaces are built using a regression method in state space. The indices are threshold strength (T) and diagonality (D). We use 48 simulated response surfaces of different shapes to test the efficacy of the indices in 3D. Our results show that T is sensitive to the steepness of the transition from one state to the next, with various forms of abrupt, centralized thresholds yielding the highest values among the simulated surfaces. D represents the orientation of the response surface or the simultaneous influence of more than one predictor in eliciting the response gradient. Strongly diagonal surfaces have the most diagonal surface area demonstrated by sharply undulating diagonal surfaces. Given that the success of T and D requires a regression method to accurately capture any shape of complex data structure, we also test the accuracy of empirical regression methods known to be tractable with complex data. We test classification and regression trees (CART), Random Forest, and non-parametric multiplicative regression (NPMR) for binary and continuous responses. We use the 48 simulated response surfaces to test the methods, and we find that prediction accuracy depends on both the T and D of the simulated data for each method. We choose the most accurate method among those we test for capturing any shape of response surface from real data, NPMR. Finally, we use NPMR to build response surfaces and quantify T and D from real ecological data sets. We demonstrate how measuring threshold strength and diagonality from multi-factor response surfaces can advance ecology.

1. Introduction

Ecological thresholds are an increasing research priority among natural, earth, and social sciences (USCCP, 2009; Andersen et al., 2009). Simply defined, ecological thresholds are a non-linear response where a small change in the input produces an abrupt change in the output for the scale at hand (USCCP, 2009; Groffman et al., 2006; Andersen et al., 2009). The occurrence of ecological thresholds can carry profound societal risks especially in the face of unprecedented environmental change (USCCP, 2009). Examples of ecological thresholds include shifts in water clarity of lakes caused from continuous nutrient loading that passes a critical point (Scheffer et al., 1993) and the conversion of arctic tundra to shrub-land triggered by a slight increase in temperature (USCCP, 2009). Such threshold behavior is common across diverse systems and scales and represents adaptive, complex behavior (Levin, 1999; Holling, 1992).

Despite their importance, the mathematical characterization of ecological thresholds is poorly developed. Current methods that quantify thresholds focus either on threshold or change-point detection in time (Andersen et al., 2009) or across geographic space (Fortin, 1994; Jacquez et al., 2000). Yet, thresholds can be represented in state space, geographic space, or time. While thresholds may be seen in time and geographic space, the direct drivers of thresholds are found in state space (Scheffer and Carpenter, 2003).

Surprisingly, few methods exist for the quantification of ecological thresholds in state space, and for those that do, most detect the location of the threshold and apply only to a single predictor (e.g. Baker and King, 2010; Brenden et al., 2008; Damgaard, 2006; Toms and Lesperance, 2003; Qian et al., 2003). In fact, to our knowledge, no method addresses the challenges that arise in state space when thresholds are characterized with respect to more than one

* Corresponding author at: Department of Botany and Plant Pathology, Oregon State University, 2082 Cordley Hall, Corvallis, OR, United States.
Tel.: +1 541 737 2312.
E-mail address: lintzh@science.oregonstate.edu (H.E. Lintz).

predictor. Given the inherent complexity of ecosystems, empirical characterization of thresholds with respect to more than one predictor (or driver) is clearly warranted (Limburg et al., 2002). The most important reason for expanding threshold analysis to multi-factor predictor domains is simple. In higher dimensional predictor space, one can detect and measure thresholds that would not be observed by analyses limited to single predictors.

One grand challenge of measuring thresholds in higher dimensional state space is that ecological thresholds can take more than one geometric form. Ecological thresholds (along with other shapes that emerge from complex systems) can result from complex behavior including interactions, hierarchical relationships, and other forms of non-linearity (Goldenfield and Kadanoff, 1999; Weng et al., 1999; Limburg et al., 2002; Kinzig et al., 2006; Andersen et al., 2009). Such complex behavior can yield many different response shapes. For example, thresholds in 3D can be oriented perpendicular or diagonal with respect to the input gradients; they can look like Niagara falls, or they can be confined to part of a response surface. Thus, the quantitative assessment of thresholds in n-dimensional state space is not as simple as fitting parametric equations, such as the logistic curve, to data. Parametric regression equations yield a distinct geometric shape or type of shape (e.g. planes or logistic curves depending on the class of equation). Consequently, by its nature, parametric regression imposes specific shapes or shape families *a priori* on data patterns. However, in complex data analysis, prudence calls for regression methods that can easily adapt to any response shape. The shape of a response surface is an emergent property of the underlying system. It warrants accurate capture, quantitative assessment, and interpretation. Unless a specific shape is expected or of interest, it should be treated as unknown prior to exploratory analysis, and ideally, exploratory analysis would use a method that does not impose a specific shape *a priori*.

An ecological threshold can be considered a type of response shape, and non-parametric regression may be the best option for assessment of multi-factor shapes or thresholds in state space. Our use of the term 'non-parametric regression' follows the definition for 'computer-intensive' regression established by Efron and Tibshirani (1991) with CART and kernel smoothers as examples. Such methods are known to be tractable with complex data and rely on computationally intensive algorithms that can involve iteration and re-sampling. Non-parametric regression may avoid imposing shape-related constraints on data patterns; however, little work tests their accuracy in recovering different shapes of response patterns. Hence, we test the prediction accuracy of non-parametric methods; particularly, we test how well they predict the true underlying shape of the data pattern. The results of this test provide us with a regression method we can use to measure shape attributes of predicted response surfaces.

Our over-arching goal is to measure the strength and orientation of multi-factor thresholds in state space. In so doing, we provide a method to verify claims of ecological thresholds and increase our understanding of the multi-factor nature of thresholds. Our method follows two general steps. First, we model a data set and generate a predictive response surface. Then, we quantify shape attributes from that surface. We are not aware of any work that quantifies shape attributes from multi-factor response surfaces as we define them.

We define threshold strength (T) as the abruptness of an ecological threshold in state space. We complement this index by measuring the orientation of thresholds with more than one predictor, something we call diagonality (D). Diagonality occurs in 3-D responses including thresholds, and its mathematical basis merits its attention in the study and interpretation of response surfaces in general. Diagonality gauges the degree to which a threshold (or

any other response shape) is influenced by more than one predictor. Diagonality can assist in identifying and describing complex interactions.

The specific research objectives of this paper are: to design indices of threshold strength and diagonality and validate them using numerous simulated data sets of different shape, to test the ability of non-parametric regression methods to recover a wide range of shapes of response structures or surfaces (including thresholds) from simulated data sets to optimize measurement of thresholds, and to provide examples of how measuring threshold strength and diagonality from real response surfaces can advance ecology.

2. Methods

2.1. Index of threshold strength

We describe our index of threshold strength for three-dimensional response surfaces in state space. We define a response surface as a uniform grid of predicted values generated using a model with continuous variables as input (Fig. 1). The response value is named z, while the two predictors are x and y. We also describe a two-dimensional version (see Appendix A). The premise of the index is based on two criteria. First, the strongest thresholds have the greatest bimodality in their frequency distribution. Second, the strongest thresholds also have the greatest monotonicity (or least change in the sign of slopes across the response surface). The second criterion is designed to rule out pathological surfaces exhibiting high bimodality but showing a spatial arrangement of response values dissimilar to a threshold.

To implement calculation of the index, the response values are divided by their maximum range to standardize among response surfaces with different ranges. We measure departure from monotonicity incrementally across the surface using a moving circular window, which we refer to as a 'spider' (Fig. 1A). Our definition of monotonicity comes from calculus, which specifies one-dimensional input. We extend the concept of monotonicity to three-dimensional response surfaces by calculating the average departure from monotonicity among repeated sets of three points as we further describe. Each set represents one-dimensional input.

To measure monotonicity from a surface of points, we use a spider comprising nine adjacent points on a grid of 100×100 increments or 101×101 points. This is a fine enough grid to capture abrupt changes in slope on a response surface. Four pairs of opposing vectors sharing a center point are defined per spider, NESW, NWSE, NS, and EW (Fig. 1A). A case definition follows for each vector pair: if the two endpoints are either both above or both below the center point, then departure from monotonicity occurs, if not, then departure from monotonicity is zero. For cases expressing departure from monotonicity, the degree of the departure follows:

$$\text{NWSE}_{i,j} = \min\left\{ \left| z_{i,j+2}^* - z_{i+1,j+1} \right|, \left| z_{i+2,j}^* - z_{i+1,j+1} \right| \right\}$$

$$\text{NESW}_{i,j} = \min\left\{ \left| z_{i+2,j+2}^* - z_{i+1,j+1} \right|, \left| z_{i,j}^* - z_{i+1,j+1} \right| \right\}$$

$$\text{NS}_{i,j} = \min\left\{ \left| z_{i+1,j+2} - z_{i+1,j+1} \right|, \left| z_{i+1,j} - z_{i+1,j+1} \right| \right\} \quad (1\text{–}4)$$

$$\text{EW}_{i,j} = \min\left\{ \left| z_{i,j+1} - z_{i+1,j+1} \right|, \left| z_{i+2,j+1} \right| \right\}$$

where z denotes a response point within a spider, and i and j index the point on a uniform grid. To give the spider a circular footprint and approximate invariance to rotation, diagonally oriented vectors are shortened through interpolation and interpolated points are denoted as z^* (Fig. 1A). See Appendix A for a description of the interpolation method. Departure from monotonicity for a spider is the sum of the departures, $S_{i,j} = \text{NWSE}_{i,j} + \text{NESW}_{i,j} + \text{NS}_{i,j} + \text{EW}_{i,j}$. The
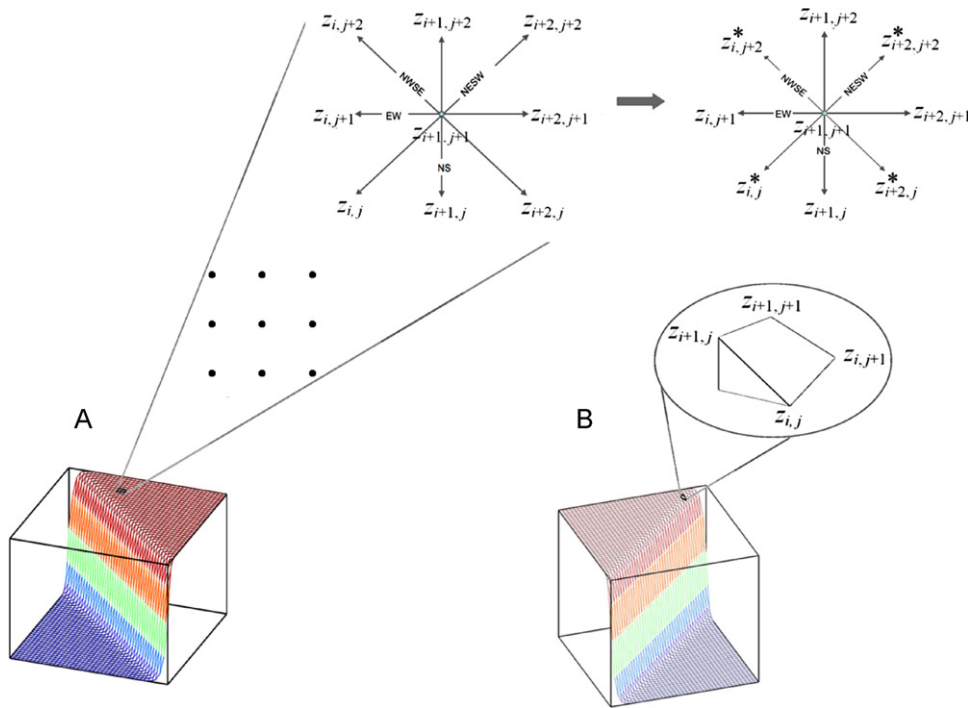
Fig. 1. (A) We calculate three-dimensional threshold strength from a modeled surface formed collectively by a grid of points. A 'spider' is established for each unique set of nine adjacent points indexed as shown. The circular spider on the right results from interpolating the diagonal vectors in the square spider on the left. Each z represents a response point, and each z^* represents an interpolated response point. Four pairs of opposing vectors are defined for each spider, NESW, NWSE, NS, and EW. (B) We demonstrate calculation of diagonality from a modeled three-dimensional surface formed collectively by many four-sided polygons defined by points as shown; the diagram to the upper right represents one polygon and illustrates indexing of the four points for calculating a metric, d, for each polygon to sum across the surface.

sum of $S_{i,j}$ across all spiders yields overall departure from monotonicity for a response surface:

$$\sum_{i=1}^{n-2}\sum_{j=1}^{n-2} S_{i,j} = \sum_{i=1}^{n-2}\sum_{j=1}^{n-2}(\mathrm{NWSE}_{i,j} + \mathrm{NESW}_{i,j} + \mathrm{NS}_{i,j} + \mathrm{EW}_{i,j}) \quad (5)$$

where n is the number of points within one predictor dimension. $\sum_{i=1}^{n-2}\sum_{j=1}^{n-2} S_{i,j}$ is divided by the total number of paired, opposing vectors for the surface (four times the total number of spiders evaluated or $4(n-2)^2$ in three-dimensions) to yield average departure from monotonicity for the surface, K. We calculate monotonicity

(M) using a negative exponential function of K, specifically:

$$M = e^{-950K} \quad (6)$$

M has a y-intercept of 1 for perfect monotonicity and an asymptote at zero for strong departures from monotonicity. We set the exponential coefficient to 950 to ensure that the low end of the range in M across 48 test surfaces (presented in Fig. 2) approaches zero for the two most undulating test surfaces. The rank order of monotonicity of the test surfaces in Fig. 2 according to M are virtually the same across three orders of magnitude of exponential coefficients that adequately detect departures from montonicity. Threshold
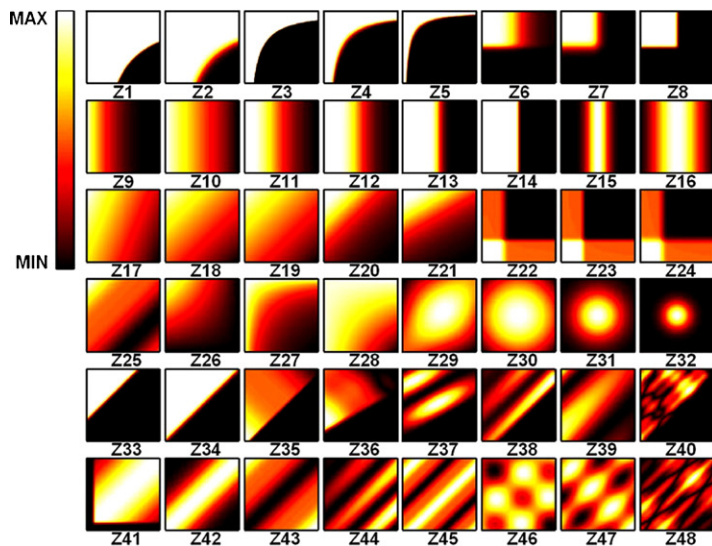

Figure 1 Legend		
Label	**Pattern name**	**Label**	**Pattern name**
Z1	steep Niagara step off-center	Z25	short stream valley
Z2	Niagara step off-center	Z26	z=xy
Z3	steep Niagara step	Z27	Niagara kite
Z4	Niagara step	Z28	z=x-xy
Z5	Niagara edge step	Z29	diag Gaussian hill-ridge
Z6	corner wave step	Z30	parachute
Z7	corner square step	Z31	Gaussian wide hill
Z8	steep corner square step	Z32	Gaussian hill
Z9	z=x³	Z33	steep diag step off-center
Z10	z=x	Z34	steep diag step
Z11	s-curve	Z35	skate-ramp abrupt diag
Z12	gentle step	Z36	Gaussian skate-ramp abrupt
Z13	moderately steep step	Z37	diag two waves abrupt
Z14	steep step	Z38	zig-zag diag abrupt
Z15	Gaussian ridge	Z39	wide zig
Z16	wide Gaussian ridge	Z40	organic peaks
Z17	z=x+0.4y	Z41	diag Gaussian ridge abrupt L
Z18	z=x+y	Z42	diag Gaussian ridge
Z19	z=0.5x+0.5y	Z43	stream valley
Z20	s-curve off-center 45	Z44	zig-zag slant
Z21	s-curve off-center 60	Z45	diag waves
Z22	triple staircase diff levels	Z46	four eggs
Z23	steep triple staircase	Z47	undulating sea
Z24	triple staircase	Z48	weaving

Fig. 2. Bird's eye views of three-dimensional 48 simulated response surfaces. Each surface is labeled to match corresponding names and index values in Table 1. The color gradient represents different values of for each response ranging from minimum to maximum as shown.

strength (T) is the product of monotonicity, M, and the bimodality of the response (Eq. (8)). The standard deviation (σ_z) measures the bimodality of the frequency distribution of the response where N is the total number of response points. The denominator is N instead of N-1 as we use the standard deviation to describe shape rather than a population sample. The standard deviation (Eq. (7)) is doubled to range from 0 to 1 (Eq. (8)). Threshold strength is simply a function of bimodality for perfectly monotonic surfaces or when monotonicity (M) is equal to one.

$$\sigma_z = \sqrt{\frac{1}{N}\sum_{i=1}^{N}(z_i - \bar{z})^2} \qquad (7)$$

$$T = 2\sigma_z M \qquad (8)$$

2.2. Index of diagonality

We define diagonality as how oblique or diagonal the gradient of a response surface is oriented relative to at least two predictor gradients. Diagonality represents the simultaneous influence of more than one predictor gradient in eliciting the response (Fig. 3A). For example, perfectly diagonal surface area represents equivalence among partial first derivatives for planes (e.g. the right-most plane of Fig. 3A). In contrast, non-diagonal planes vary strictly with one predictor (e.g. the left-most plane of Fig. 3A). Further, surfaces with traditional, statistical interactions create curvature and thus some diagonality (for example, regression models containing multiplicative terms in an additive model) (Fig. 3B), but diagonal surfaces need not have statistical interactions (e.g. the right-most plane of Fig. 3A). Statistical interactions occur when the effect of one pre-
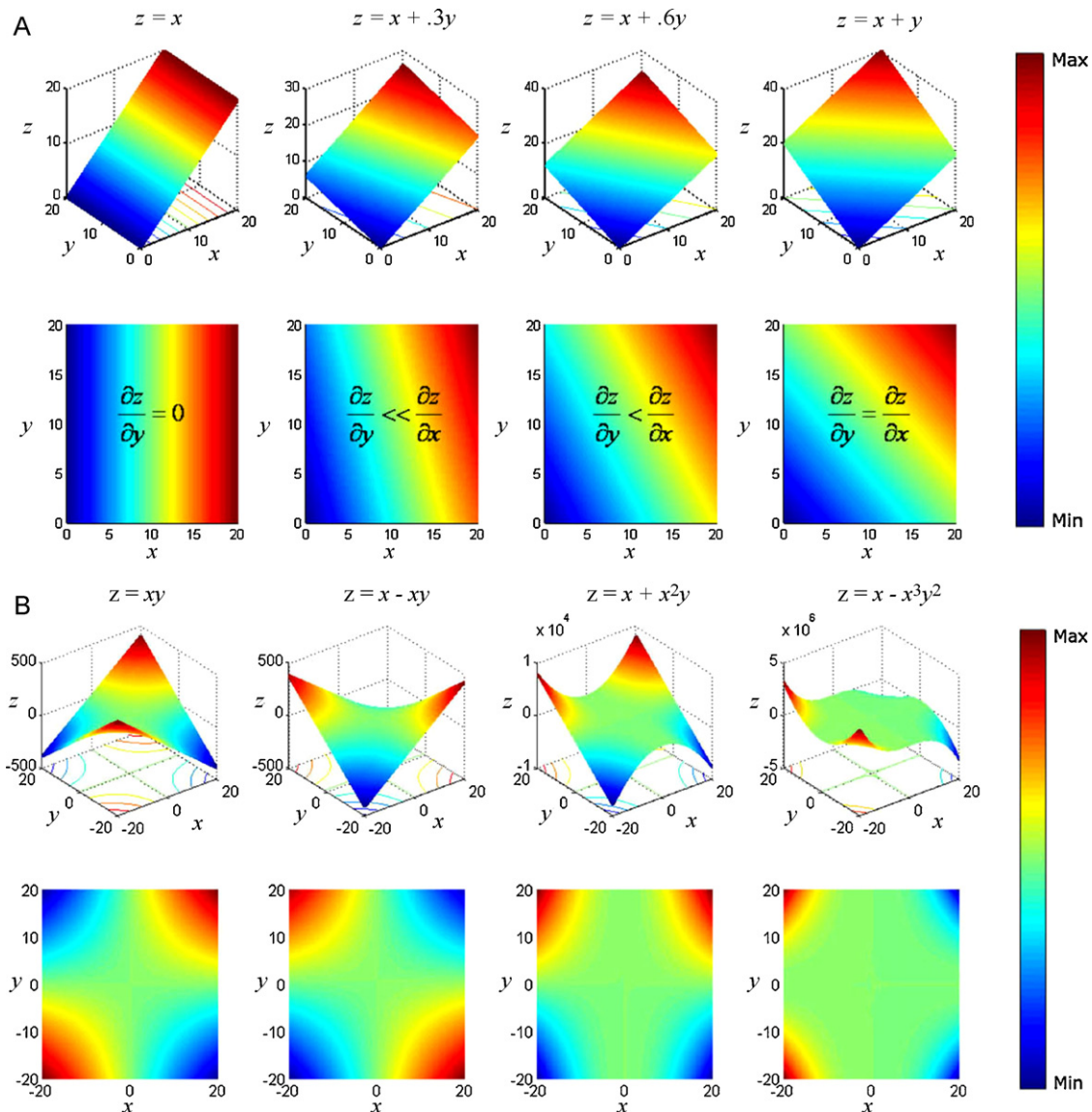

Fig. 3. (A) Four three-dimensional planes (top row) with each generating function (titled above) and matching bird's eye views (bottom row). The planes increase in diagonality from left to right. Perfectly diagonal surface area (e.g. the right-most plane) represents equivalence among partial first derivatives. In contrast, non-diagonal surface area varies strictly with one predictor (e.g. the left-most plane). In between the extremes, the rate of change of z with respect to y gradually becomes more important until it reaches equivalence with the rate of change of z with respect to x for a diagonal plane. (B) Four three-dimensional response structures (top row) with each generating function (titled above) and matching bird's eye views (bottom row). Each function represents a different additive, statistical model containing an interaction term or, in this case, a multiplicative term comprising predictors x and y. The details of the four additive models vary; in particular, the functions are a mix of different orders. The four structures capture the shape family of additive models with multiplicative terms, hyperbolic paraboloids. Despite the details of the additive model and multiplicative terms, the equations yield similar shapes. Interactions of this sort create curvature and thus some diagonality but strongly diagonal surfaces such as diagonal planes need not have statistical interactions.

dictor on a response depends on values of another predictor or predictors.

Diagonality (*D*) is calculated for a three-dimensional response surface formed by a grid of 101 by 101 points. The grid is comprised of many four-sided polygons each defined by a unique set of four adjacent points (Fig. 1B). The vertical distance between diagonally opposed points is calculated for each polygon, and the absolute difference between these two vertical distances is termed d_g, where g indexes a single polygon.

$$d_g = \left| \left| z_{i,j+1} - z_{i+1,j} \right| - \left| z_{i,j} - z_{i+1,j+1} \right| \right| \tag{9}$$

Pure diagonality (*P*) is the sum of d_g across the total number of polygons (*q*). *P* is divided by the standard deviation of the response (σ_z from Eq. (7)) for comparison among disparate surfaces to yield *H* or standardized pure diagonality. *H* increases linearly with the square root of *q*; hence, it is divided by the square root of *q* to yield diagonality, *D*, a variable insensitive to *q*:

$$D = \frac{H}{\sqrt{q}} \tag{10}$$

2.3. Simulated data

We test the indices with simulated data sets representing varying degrees of threshold strength and diagonality common to ecological data in state space (Table 1, Fig. 2). Our choice of simulated data emerges from theoretical expectations of ecological response surfaces (e.g. Scheffer and Carpenter, 2003; Austin, 2007), published examples where shapes are unconstrained by modeling methods (e.g. Waring and Major, 1964; Makarewicz and Likens, 1975; Bartlein et al., 1986), and author experience with hundreds of ecological response surfaces. Also, several data sets are included to expand the diagonality gradient (e.g. Z46, Z47, and Z48 in Fig. 2). Although several data sets appear quite similar (Z22, Z23, and Z24 in Fig. 2), they have subtle yet important differences in steepness and step height.

2.4. Method comparison

We test the performance of each of three methods in modeling 48 simulated data sets as continuous and binary data. We select different classes of non-parametric regression methods known to be tractable with complex data (Efron and Tibshirani, 1991): classification and regression trees (CART) (Breiman et al., 1984), non-parametric multiplicative regression (NPMR) (a kernel smoother) (McCune, 2006), and a statistical ensemble method using CART as a building block, Random Forest (Breiman, 2001). For each method we use the same settings across all test surfaces. We establish settings from recommendations and examples in peer-reviewed literature (explanations of methods and settings are described in Appendix A).

We compare the prediction accuracy (henceforth referred to as accuracy) of the methods by examining prediction error across all simulated shapes for binary and continuous responses. The accuracy for a continuous response is assessed with R^2. For accuracy in binary classification, we use the area under the receiver operator characteristic curve (AUC) (see Appendix A) (Hanley and McNeil, 1982). Fig. 4 depicts scatterplots of accuracy versus threshold strength and diagonality for CART, Random Forest, and NPMR. Each point represents a median, externally validated accuracy of 100 models built from random samples (*N* = 250), which are drawn from a simulated data set (100 increments squared or size *N* = 10,201) of specific shape; we choose *N* = 250 as a realistic size for an ecological data set. External validation gauges prediction error for external data. We rely on variable selection and overfitting controls inherent to each method when supplied with the two predictors (*x*, *y*).

3. Results

3.1. Efficacy of the threshold strength index

The rank order of threshold strength is sensitive to steepness or how closely the response surfaces resemble a single step with highly undulating surfaces yielding the lowest threshold strength (*T* = 0), progressing through the Gaussian hill (*T* = 0.36) to the Gaussian ridge (*T* = 0.68) to end with various forms of strong, centralized thresholds (*T* > 0.93) (Table 1, Fig. 2). All surfaces with morphologies resembling single steps rank higher than the other shapes presented. The index tracks incremental changes in steepness among similarly shaped monotonic surfaces such as single steps (e.g. Table 1, Z1 and Z2 in Fig. 2; see Appendix A); however, increased departure from monotonicity can slightly increase with increased steepness in 'staircases' (Z24 > Z23 in Fig. 2); yet, the effect of this is not detectable at two decimal places. The index ranks surfaces resembling centralized steps similarly regardless of exact form. Thus, a central threshold showing a steep transition albeit with more curvature (from a bird's eye view) (e.g. Z3) ranks closely with a central step showing a steep transition but no curvature (e.g. Z34) (Table 1, Fig. 2). The general shape of a threshold (albeit with variable steepness) is lost below *T* = 0.72 for the sample of 48 shapes we provide (Table 1, Fig. 2). Additionally, surfaces in two and three dimensions generated from the same function yield equivalence in threshold strength (see Appendix A). Finally, the index detects abrupt changes between planar features that are parallel to the *x*–*y* plane. For example, the surface Z35 contains an abrupt change between different regions of the response surface where one side of the transition is *z* = 0 (or a static value for the response variable shown as a single color, black) but the other side of the transition resembles a skate ramp (shown with the color gradient; Fig. 2). Consequently, Z35 yields a relatively low value of threshold strength (*T* = 0.53). Although an abrupt transition exists in this surface, the transition does not contribute to a step-like form where each state is flat and parallel to the *x*–*y* plane, which is the operational definition of a threshold we present here.

3.2. Efficacy of the diagonality index

The simulated 3D surfaces varying with only one predictor have diagonality of zero as expected (Table 1). Strongly diagonal surfaces have the most diagonal surface area demonstrated by sharply undulating diagonal surfaces such as 'weaving' (*D* = 20.31) (Z48 in Fig. 2). The index is insensitive to scale for scales small enough to capture global shape starting with 100 increments or 101 by 101 points for a square grid. Also, diagonality varies linearly with angle of rotation for a surface as expected (see Appendix A). However, the index does not explicitly discern the spatial location and configuration of diagonality present within a surface. For example, two different shapes of surfaces, one planar (Z17, Fig. 2) and another kite-like (Z27, Fig. 2) have very similar values of diagonality (*D* = 2.55, and *D* = 2.52 respectively).

3.3. Accuracy of modeling methods with simulated data

The accuracy of each method depends on the threshold strength and diagonality of the original data structure with each method differing in degree of dependence (Fig. 4). The accuracy of most methods decreases as diagonality increases and threshold strength decreases with the exception of NPMR with continuous data (lower right two axes, Fig. 4). NPMR demonstrates the least variability (seen as quantile bars in Fig. 4) and the greatest accuracy (seen as medians in Fig. 4) compared to the other methods for a given response shape. The sensitivities of modeling methods to shape attributes of data structure arises from features specific to each

Table 1
Simulated data surfaces from Fig. 2 named and ranked in descending order by values of diagonality (D) (left panel) and threshold strength (T) (right panel).

D	Label	Surface name	T	Label	Surface name
20.31	Z48	Weaving	0.980	Z14	Steep step
16.15	Z45	Diag waves	0.963	Z3	Steep Niagara step
15.29	Z44	Zig-zag slant	0.961	Z34	Steep diag step
13.36	Z38	Zig-zag diag abrupt	0.936	Z4	Niagara step
11.03	Z40	Organic peaks	0.931	Z13	Moderately steep step
9.12	Z47	Undulating sea	0.846	Z33	Steep diag step off-center
8.58	Z43	Stream valley	0.805	Z1	Steep Niagara step off-center
7.71	Z37	Diag two waves abrupt	0.801	Z12	Gentle step
7.63	Z42	Diag Gaussian ridge	0.781	Z5	Niagara edge step
6.17	Z39	Wide zig	0.772	Z8	Steep corner square step
5.96	Z30	Parachute	0.770	Z7	Corner square step
5.90	Z25	Short stream valley	0.757	Z2	Niagara step off-center
5.31	Z46	Four eggs	0.727	Z11	s-Curve
4.93	Z29	Diag Gaussian hill-ridge	0.716	Z6	Corner wave step
4.85	Z18	$z = x + y$	0.676	Z15	Gaussian ridge
4.85	Z19	$z = 0.5x + 0.5y$	0.673	Z16	Wide Gaussian ridge
4.65	Z35	Skate-ramp abrupt diag	0.623	Z41	Diag Gaussian ridge abrupt L
4.64	Z31	Gaussian wide hill	0.618	Z42	Diag Gaussian ridge
4.42	Z20	s-Curve off-center 45	0.597	Z24	Triple staircase
4.14	Z36	Gaussian skate-ramp abrupt	0.597	Z22	Triple staircase diff levels
4.05	Z34	steep diag step	0.596	Z23	Steep triple staircase
3.73	Z32	Gaussian hill	0.583	Z10	$z = x$
3.69	Z41	Diag Gaussian ridge abrupt L	0.576	Z21	s-Curve off-center 60
3.35	Z33	Steep diag step off-center	0.575	Z9	$z = x^3$
3.14	Z21	s-Curve off-center 60	0.569	Z27	Niagara kite
2.99	Z26	$z = xy$	0.554	Z20	s-curve off-center 45
2.9	Z28	$z = x - xy$	0.528	Z35	Skate-ramp abrupt diag
2.55	Z17	$z = x + 0.4y$	0.500	Z31	Gaussian wide hill
2.52	Z27	Niagara kite	0.454	Z29	Diag Gaussian hill-ridge
2.37	Z2	Niagara step off-center	0.449	Z17	$z = x + 0.4y$
2.25	Z1	Steep Niagara step off-center	0.448	Z30	Parachute
1.94	Z4	Niagara step	0.445	Z26	$z = xy$
1.89	Z3	Steep Niagara step	0.443	Z25	Short stream valley
1.77	Z5	Niagara edge step	0.426	Z28	$z = x - xy$
0.37	Z6	Corner wave step	0.421	Z43	Stream valley
0.36	Z24	Triple staircase	0.412	Z18	$z = x + y$
0.34	Z7	Corner square step	0.412	Z19	$z = 0.5x + 0.5y$
0.26	Z22	Triple staircase diff levels	0.409	Z39	Wide zig
0.21	Z23	Steep triple staircase	0.365	Z32	Gaussian Hill
0.10	Z8	Steep corner square step	0.362	Z36	Gaussian skate-ramp abrupt
0.00	Z14	Steep step	0.336	Z37	Diag two waves abrupt
0.00	Z12	Gentle step	0.280	Z46	Four eggs
0.00	Z13	Moderately steep step	0.220	Z38	Zig-zag diag abrupt
0.00	Z11	s-Curve	0.215	Z44	Zig-zag slant
0.00	Z16	Gaussian ridge	0.198	Z47	Undulating sea
0.00	Z15	Wide Gaussian ridge	0.122	Z45	Diag waves
0.00	Z10	$z = x$	0.000	Z40	Organic peaks
0.00	Z9	$z = x^3$	0.000	Z48	Weaving

modeling method, which manifest in visual differences of predicted surfaces for different shapes (Fig. 5). For our subsequent analyses using real ecological data, we choose the most accurate and robust method we test, NPMR. Additionally, we append the simulated data sets underlying the surfaces shown in Fig. 2 (see Appendix D Supplements 1 through 3). We encourage testing of other methods.

3.4. Application of the indices

Application of threshold strength and diagonality with real data can test theory and answer questions about ecological thresholds. We present examples using real data with the goal of demonstrating how the indices can be applied (Fig. 6). The results provided by the examples are preliminary and require further investigation. Our examples focus on thresholds in state space. However, we recognize that these tools can apply to thresholds in time and geographic space, and these are topics of future study.

For our first example, the indices evaluate the theory formulated by Berryman (1982) and reviewed by Christiansen et al. (1987) (Fig. 6A). The theory holds tree vigor and bark beetle attack

as drivers of threshold responses in tree or stand survival across species. Here we evaluate the question, do bark beetle densities and tree vigor drive threshold responses in sapwood survival across tree species? Fig. 6A demonstrates that the response surface of *Picea abies* survival has a moderately strong threshold (T = 0.76), while *Pinus contorta* has a weaker threshold (T = 0.61). For benchmark comparisons, see surface Z2, Fig. 2, Table 1, also with T = 0.76, and a diagonally tilted plane, Z19, with T = 0.41. The results suggest that the theory does not apply equally well to both species for the variables tested. Also, responses of both species show diagonality; thus, each surface demonstrates that both factors elicit the response gradient among species. However, *P. abies* shows greater diagonality compared to *P. contorta* (Fig. 6A). Other factors likely need to be given account as recent works support cross-scale drivers behind bark beetle thresholds (e.g. Raffa et al., 2005, 2008).

Fig. 6B demonstrates an application of threshold strength in a 2D context. Since this is in 2D, only threshold strength can be measured. For this example we ask: does greater stomatal control (termed isohydry) create stronger thresholds in percent loss of conductivity versus water potential for woody vascular plants?
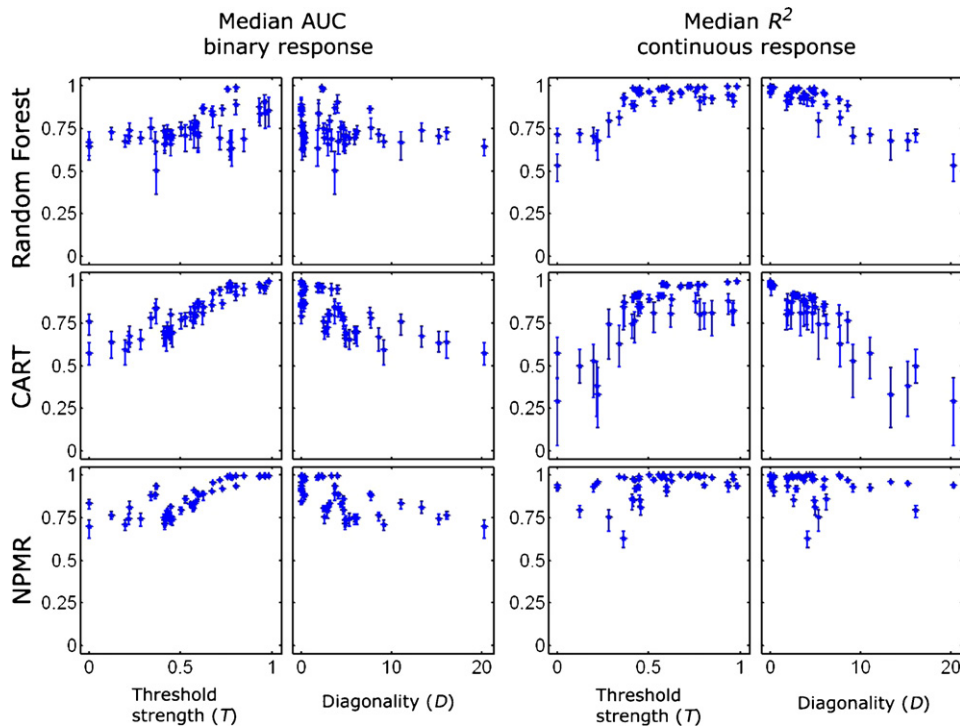
Fig. 4. Prediction accuracy of Random Forest, Classification and Regression Trees (CART), and non-parametric multiplicative regression (NPMR) for continuous and binary responses plotted versus threshold strength (T) and diagonality (D). Each point is a median, externally validated accuracy of 100 models built from random samples size where $N = 250$. The samples draw from a large subset of a simulated data set ($N = 9201$). A separate subset of 1000 points performs external validation for each simulated data set (see Fig. 2 for the simulated data sets). Error bars represent 95% quantiles.

Isohydric plants close their stomata (cells controlling gas exchange from leaves) when leaf water potentials reach a set value. Anisohydric plants allow water potential to decline with water stress (Vogt, 2001). Vulnerability curves measure the percent loss of hydraulic

Fig. 5. A visual comparison of predicted three-dimensional response surfaces together with surfaces showing the original data (bird's eye views). Results are shown from three modeling methods for two types of responses, continuous and binary. In the case of the right-most three columns, the binary response surfaces represent the probabilities of underlying point densities. The top row depicts the original response surfaces each comprising 10,201 data points or 100 by 100 increments. The lower rows show predicted values for models built from a random subsample (size $N = 250$) of each original response surface in the top row. Two replications of random samples are shown for each modeling method to provide a sense of the variation.

conductivity of xylem (water-conducting tissue) with declining water potential; they also assess the function of water-transporting conduits within the plant during drought stress (Sperry et al., 1988) (Fig. 6B). Isohydry may create stronger thresholds in vulnerability curves of vascular plants as the strategy precludes the need for plants to construct conduits with differing resistances to water stress. The measurement of threshold strength from vulnerability curves of iso- or aniso-hydric species is necessary to evaluate the research question. Preliminary calculations suggest that increased stomatal control may create stronger thresholds in vulnerability curves ($T = 0.82$, 0.74 for isohydric species; $T = 0.62$, 0.58 for anisohydric species) (Fig. 6B). However, a larger sample size consisting of more species is needed to ascertain this.

Last, threshold strength and diagonality can be applied to selected domains within a complex response surface. For example, Fig. 6C shows a cropped portion of a response surface for a model of the probability of tree species' occurrence relative to climate for *Pinus ponderosa* in Oregon. The model is based on presence/absence data (Azuma et al., 2002, 2004). We select and crop the response within a specific climate domain. At first glance, one might assume that the selected portion of the response surface resembles a threshold; however, when compared to simulated data, the threshold strength is weak ($T = 0.68$). Further, the low diagonality shows that the response within this domain is mainly driven by a single variable ($D = 0.76$). However, the diagonality of the surface as a whole demonstrates that both drivers are responsible for eliciting the response gradient (mostly in regions outside the selected domain) ($D = 5.41$). The lack of diagonality within the cropped domain in Fig. 6C elicits the following question: why is the probability of tree species occurrence only attributable to PCA1 within the selected domain? Response surfaces are snapshots of complex system behavior, and quantifying the diagonality (and threshold strength) of selected regions of response surfaces can identify interactions within the surfaces.
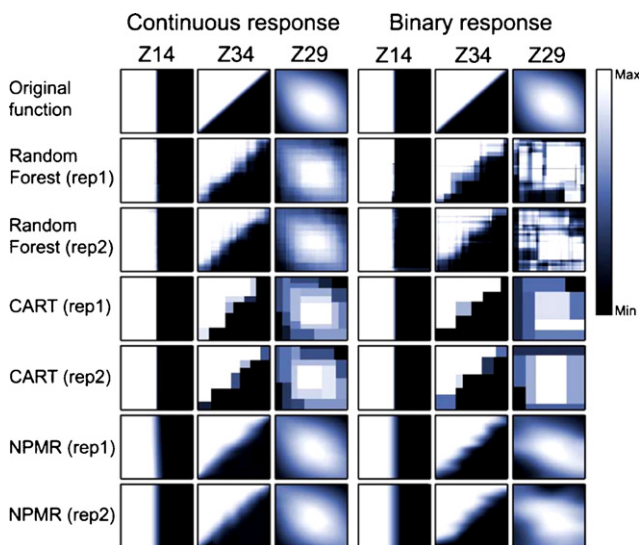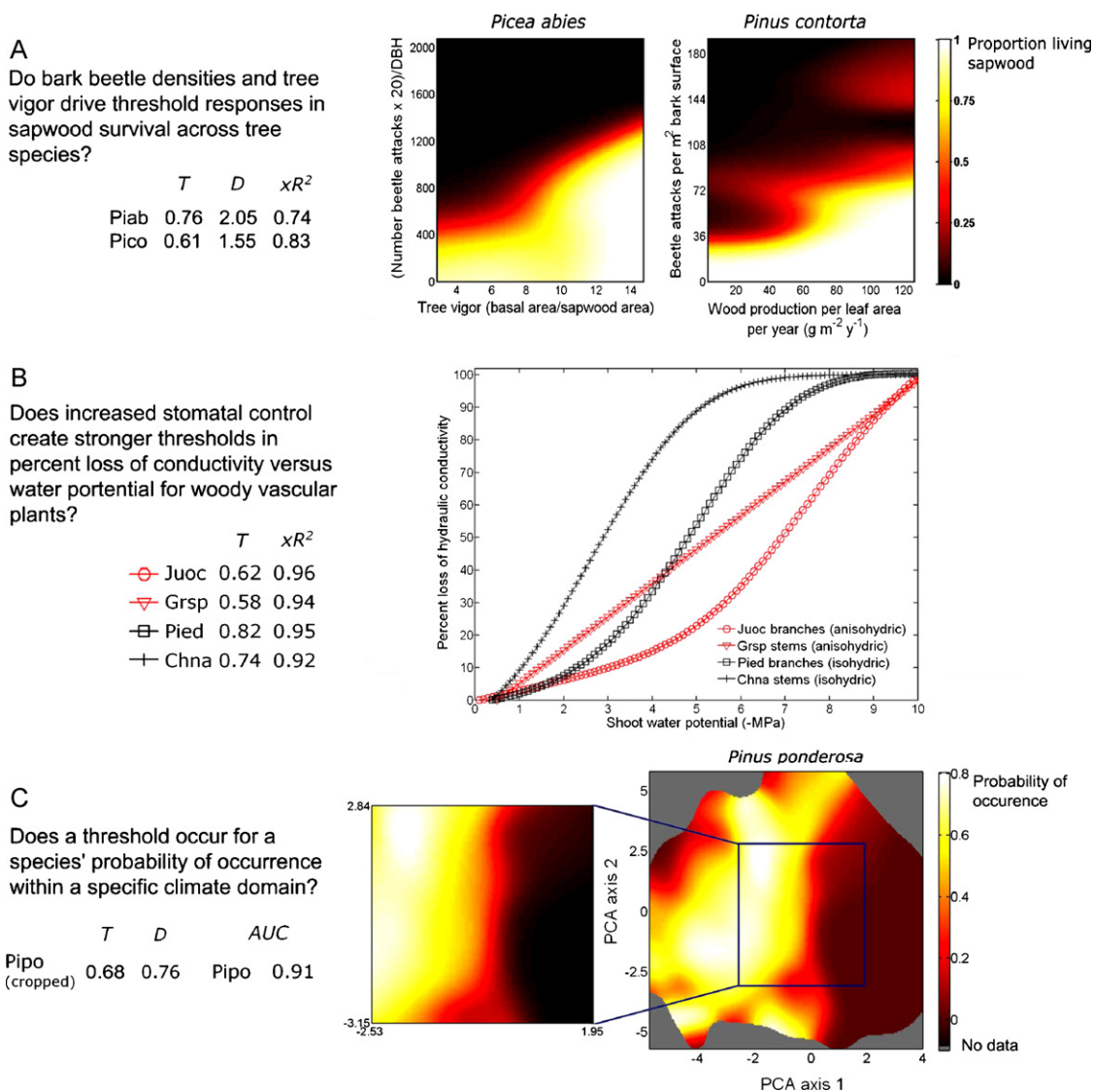
Fig. 6. The application of threshold strength (T) and diagonality (D) to ecological data using prediction surfaces (right) generated by NPMR for different data sets (see Appendix B: Table B1 for specifications). Threshold strength (T) and diagonality (D) values (left) are measured from modeled surfaces (right) test different questions (left). (A) Proportion of sapwood survival versus separate measures of tree vigor and severity of bark beetle attack for two tree species. Left: *Picea abies* attacked by *Ips typographus*. Right: *Pinus contorta* attacked by *Dendroctonus ponderosae*; data and theory from (Christiansen et al., 1987). (B) Mean percent loss in hydraulic conductivity versus shoot water potential (−MPa) of branches of two isohydric (red lines) and two anisohydric (black lines) species. Lines show predicted curves from data of stems of two shrub species, *Grayia spinosa* and *Chrysothamnus nauseosus* (Hacke et al., 2000), and branches of two tree species *Juniperus osteosperma* and *Pinus edulis* (Linton et al., 1998) (see Appendix C: Fig. C1). (C) Probability of occurrence for a dominant tree species in Oregon, *Pinus ponderosa*, modeled relative to two axes derived using Principal Components Analysis. A summer aridity gradient (axis 2) increases vertically and a continentality gradient (axis 1) increases from right to left (see Appendix C: Fig. C2). Together, the axes explain 82% of variability in the source data (see Appendix B: Table B2). Threshold strength and diagonality are measured from a cropped portion of the surface (middle). Data come from 1724 plots of the Forest Inventory Analysis program in Oregon (Azuma et al., 2002, 2004). (For interpretation of the references to colour in this figure legend, the reader is referred to the web version of the article.)

4. Discussion

4.1. Ecological relevance

Threshold strength and diagonality represent the first tools to quantify multi-factor ecological thresholds in state space. The examples with real data demonstrate utility of the indices in state space. For example, we measure threshold strength for a diagonal response in multi-factor state space (e.g. Fig. 6A, left panel). We detected a relatively strong threshold. If this response data were to be analyzed with respect to either one of those predictors alone, the threshold strength would be much lower.

The indices can be measured from a cropped portion of a response surface. This is a fundamental step toward using the indices within a roving window to measure T and D at different scales within the surface (Fig. 6C). This can serve various research purposes such as finding the regions of strong behavior in a multi-factor response surface. Finally, this approach can be generalized into asking what conditions affect strength of a threshold in state space. Answering this question can provide insight into mechanism.

4.2. Statistical relevance

Each empirical modeling method we test recovers data structure using a 'building material' specific to the algorithm. By analogy, CART uses square or rectangular prisms, Random Forest tends to stipple with long narrow rectangular prisms, and NPMR uses smooth, stretchy material (see Fig. 5). Model building algorithms can introduce substantial model bias when the geometric con-

straints of building material are not suited to the shape of the response. For example, CART's building material, square and rectangular prisms, inefficiently captures diagonal gradients. Overall, CART performs better with non-diagonal thresholds by splitting data at threshold values and creating discrete prediction levels for subsets of predictor values. This maintains square, flat areas typical of non-diagonal thresholds or thresholds responding to a single predictor (Fig. 5). CART models can be 'pruned' numerous ways (Hastie and Tibshirani, 2001), which change the size of the prisms and hence sensitivity to diagonality. However, our method of pruning using ten-fold cross-validation is the most objective and robust to external data (Hastie and Tibshirani, 2001), yet, this process creates large prisms.

Random Forest also uses rectangular prisms as building material but the prisms are typically much narrower and longer compared to CART. Diagonality challenges Random Forest the same way it challenges CART. Rectangular prisms inefficiently capture the diagonal faces while efficiently capturing large, rectangular, flat areas typical of non-diagonal thresholds (see Fig. 5).

NPMR produces smooth renditions of response patterns, and the sensitivity of the method to threshold strength and diagonality is not due to the geometric constraints of the predictions. The sensitivity of NPMR to threshold strength and diagonality is likely due to the decrease in accuracy of predictions occurring when sloping surfaces abut the edges of the predictor space. The smoothing function biases the edges toward the central tendency of the data. The degree of this bias depends on the type of smoothing function and the width of the kernel per predictor. Broader kernels incur more bias.

In summary, non-parametric regression methods vary in their efficacy of capturing response shapes. They are sensitive to the threshold strength and diagonality of the underlying surface. The contribution of tests that use threshold strength and diagonality is especially relevant to the comparisons of empirical methods designed for complex data analysis such as species-habitat models in ecology (e.g. Elith et al., 2006; Guisan et al., 2007). Currently, methods are compared using real data sets of unknown structure, and the comparisons do not discern the role of the response shape in method performance (e.g. Elith et al., 2006; Guisan et al., 2007). Our work shows that non-parametric regression approaches can impose substantial model bias, and this bias depends on the geometry of the algorithm's 'building blocks' coupled with the geometry of the data structures. For example, the accuracy of CART is highest with non-diagonal shapes and lowest for diagonal shapes of data structure. The error or bias incurred from the limits of CART's algorithm is more pronounced for strongly diagonal surfaces. Strongly diagonal surfaces are not amenable to capture by rectangular prisms (the analytical type of 'building block' imposed by the algorithm). Such model bias has unknown and possibly far-reaching consequences across disciplines that apply these methods. Other disciplines using these methods range broadly from epidemiology to earth sciences.

4.3. Methodological considerations

We measure threshold strength and diagonality on a continuous scale rather than assigning a simple 'yes' or 'no'. Values for threshold strength can be interpreted by comparison to our benchmarks (the shapes represented among the 48 simulated data sets; Table 1, Fig. 2) or by comparison among data sets.

Because our simulated gradients represent many possible response surfaces, T and D can be applied to any ecological regression with one or two continuous predictors. T and D depend on how well the shape of the response surface is sampled and fit. All of our examples with real data involve well-sampled response surfaces with strong fits. Fig. 6A and B shows examples with con-

tinuous response (or dependent) variables, and Fig. 6C shows a binary response variable. The indices can be used with response surfaces modeled in state space from other disciplines. An important exception includes surfaces where more than one response value corresponds to a single unique combination of input values. A classic example of this comes from the cusp catastrophe of catastrophe theory where a surface in state space exhibits a cusp-like fold in the ordinate or z-dimension of an x, y, z coordinate system (Thom, 1989). Although the cusp catastrophe surface is not generated using regression, it is still a surface in state space, albeit theoretical. Folds in the ordinate dimension of state space can exist empirically and theoretically. However, regression methods cannot capture such folds, and the indices we present are not equipped to measure such folds.

Although we limit the index development to three dimensions of state space, the indices are specifically designed for ease of algebraic extension to n-dimensions of state space. Evaluation of multi-factor thresholds in more than three dimensions of state space would offer more realism to threshold analysis. Extension of the indices to n-dimensions of state space is a topic of future research. Finally, the indices are not equipped to measure the relative importance among predictors in eliciting a threshold in state space. However, this is can be measured using statistics from non-parametric modeling methods. For example, in NPMR, "sensitivity" is a measure of relative variable importance.

4.4. Geographic relevance

The indices of threshold strength and diagonality may conceivably be used in domains other than state space such as geographic. Thresholds in the geographic domain are considered 'boundaries' or transition zones that delineate patches (Cadenasso et al., 2003). Boundaries in a geographic domain can be visualized as meandering zones of abrupt change differing in extent and magnitude, and the objective is to map and characterize these meanders across space. Employing threshold strength (presented here) incrementally within a window at a fixed resolution in geographic space may be appropriate for some applications. In fact, an algorithm measuring abruptness of geographic boundaries in ecology already exists (Bowersox and Brown, 2001) based largely on the work of Fortin (1994) and Womble (1951); however, this algorithm does not provide a value of threshold abruptness that is insensitive to rotation with respect to longitude and latitude (or the analogous x–y plane). We explain this and the associated significance below.

First, boundary mapping employed by Fortin (1994) and Womble (1951) identifies abrupt change across a spatial grid of points by employing arbitrary cut-off values in the absolute values of partial first derivatives among adjacent points. The identified steep slopes and their spatial locations are called boundary elements. Bowersox and Brown (2001) build on boundary elements to develop a method to measure the abruptness of such a boundary. They measure the area under the curve representing a frequency distribution of boundary elements using a gradient of twenty different cut-off values. The idea is that strong thresholds will show a spike in numbers of boundary elements with high cut-offs. This makes a taller, narrower curve with a longer tail compared to other curves. However, partial first derivatives change across the same point pattern but rotated 45°, and consequently, they are not rotationally invariant in the x-y plane. Hence, the same boundary rotated 45° will yield different magnitudes of partial first derivatives tied to each boundary element. Further, the metric is not spatially explicit and does not distinguish a threshold shape from a different shape with the same frequency distribution of boundary elements.

In contrast, our threshold strength index solves these problems. Our criteria of monotonicity (Eq. (6)) and bimodality (the left

multiplicand equation (8)) together describe the characteristic of the shape as a whole. The criteria distinguish abrupt thresholds from less abrupt thresholds, or abrupt thresholds from shapes with no thresholds, and so on, regardless of their orientation in the x–y plane.

5. Conclusion

Threshold strength and diagonality are measurable shape attributes of multi-dimensional thresholds. We provide new tools to quantify this underused type of information. The shape of a data pattern is fundamental to the development of theory in ecology (e.g. Whittaker, 1975); yet, shortfalls in the description and understanding of a complex response shapes may be pervasive. These shortfalls can impede theoretical advancement, successful prediction, and management application (Efron and Tibshirani, 1991; Scheffer and Carpenter, 2003).

We move beyond single-factor methods of quantifying thresholds that occur in state space to add realism and higher dimensionality. We introduce a parameter-free way to quantify threshold strength and diagonality from thresholds occurring in state space. Future methodological and basic research objectives for the indices include: to measure if and how the prediction accuracy of other non-parametric regression methods depends on T and D, to develop a roving window method that can measure the indices at different scales within a response surface, to study mechanisms underlying multi-factor thresholds for ecological systems hypothesized to exhibit thresholds, and to answer the question, how can this approach be used to identify systems approaching threshold responses before they happen?

Acknowledgements

Appendix A. Supplementary data

Supplementary data associated with this article can be found, in the online version, at doi:10.1016/j.ecolmodel.2010.10.017.

References

Andersen, T., Cartensen, J., Hernández-Garcia, E., Duarte, C.M., 2009. Ecological thresholds and regime shifts: approaches to identification. Trends Ecol. Evol. 24, 49–57.
Austin, M., 2007. Species distribution models and ecological theory: a critical assessment and some possible new approaches. Ecol. Model. 200, 1–19.
Azuma, D.L., Bednar, L.F., Hiserote, B.A., Veneklase, C.A., 2004. Timber Resource Statistics for Western Oregon, 1997. USDA Forest Service Pacific Northwest Research Station Resource Bulletin PNW-RB-237 (revised).
Azuma, D.L., Dunham, P.A., Hiserote, B.A., Veneklase, C.A., 2002. Timber Resource Statistics for Eastern Oregon, 1999. USDA Forest Service Pacific Northwest Research Station Resource Bulletin PNW-RB-238.
Baker, M.E., King, R.S., 2010. A new method for detecting and interpreting biodiversity and ecological community thresholds. Methods Ecol. Evol. 1, 25–37.
Bartlein, P.J., Prentice, I.C., Webb, T., 1986. Climatic response surfaces from pollen data for some eastern North American taxa. J. Biogeogr. 13, 35–57.
Berryman, A.A., 1982. Biological control, thresholds and pest outbreaks. Environ. Entomol. 11, 544–549.
Bowersox, M.A., Brown, D.G., 2001. Measuring the abruptness of patchy ecotones—a simulation-based comparison of landscape pattern statistics. Plant Ecol. 156, 89–103.
Breiman, L., Friedman, J.H., Olshen, R.A., Stone, C.J., 1984. Classification and Regression Trees. Chapman and Hall, New York, USA, p. 358.
Breiman, L., 2001. Random forests. Mach. Learn. 45, 5–32.
Brenden, T.O., Wang, L., Su, Z., 2008. Quantitative identification of disturbance thresholds in support of aquatic resource management. Environ. Manage. 42, 821–832.

Cadenasso, M.L., Pickett, S.T.A., Weathers, K.C., Jones, C.G., 2003. A framework for a theory of ecological boundaries. Bioscience 53, 750–758.
Christiansen, E., Waring, R.H., Berryman, A.A., 1987. Resistance of conifers to bark beetle attack: searching for general relationships. Forest Ecol. Manage. 22, 89–106.
Damgaard, C., 2006. Modelling ecological presence-absence data along an environmental gradient: threshold levels of the environment. Environ. Ecol. Stat. 13, 229–236.
Efron, B., Tibshirani, R., 1991. Statistical data analysis in the computer age. Science 253, 390–395.
Elith, J., Graham, C.H., Anderson, R.P., Dudik, M., Ferrier, S., Guisan, A., Hijmans, R.J., Huettman, F., Leathwick, J.R., Lehmann, A., Li, J., Lohmann, L., Loiselle, B.A., Manion, G., Moritz, C., Nakamura, M., Nakazawa, Y., Overton, J.M., Peterson, A.T., Phillips, S., Richardson, K., Pereira, R.S., Schapire, R.E., Soberon, J., Williams, S.E., Wisz, M., Zimmermann, N.E., 2006. Novel methods improve predictions of species' distributions from occurrence data. Ecography 29, 129–151.
Fortin, M., 1994. Edge detection algorithms for two-dimensional ecological data. Ecology 75, 956–965.
Goldenfield, N., Kadanoff, L.P., 1999. Simple lessons from complexity. Science 284, 87–89.
Groffman, P.M., Baron, J.S., Blett, T., Gold, A.J., Goodman, I., et al., 2006. Ecological thresholds: the key to successful environmental management or an important concept with no practical application? Ecosystems 9, 1–13.
Guisan, A., Zimmerman, N.E., Elith, J., Graham, C.H., Phillips, S., Peterson, A.T., 2007. What matters for predicting the occurrences of trees: techniques, data, or species' characteristics? Ecol. Monogr. 77, 615–630.
Hacke, U.G., Sperry, J.S., Pittermann, J., 2000. Drought experience and cavitation resistance in six shrubs from the Great Basin. Utah Basic Appl. Ecol. 1, 31–41.
Hanley, J.A., McNeil, B.J., 1982. The meaning and use of the area under a receiver operating characteristic (ROC) curve. Radiology 143, 29–36.
Hastie, T., Tibshirani, R., 2001. The Elements of Statistical Learning. Springer, New York, p. 524.
Holling, C.S., 1992. Cross-scale morphology, geometry, and dynamics of ecosystems. Ecol. Monogr. 62, 447–502.
Jacquez, G.M., Maruca, S., Fortin, M.J., 2000. From fields to objects: a review of geographic boundary analysis. J. Geogr. Syst. 2, 221–241.
Kinzig, A.P., Ryan, P., Etienne, M., Allison, H., Elmqvist, T., Walker, B.H., 2006. Resilience and regime shifts: assessing cascading effects. Ecol. Soc. 11, 20–36.
Levin, S., 1999. Fragile Dominion: Complexity and the Commons. Perseus Books, Massachusetts, p. 250.
Limburg, K.E., O'Neill, R., Costanza, R., Farber, S., 2002. Complex systems and valuation. Ecol. Econ. 41, 409–420.
Linton, M.J., Sperry, J.S., Williams, D.G., 1998. Limits to water transport in Juniperus osteosperma and Pinus edulis: implications for drought tolerance and regulation of transpiration. Funct. Ecol. 12, 906–911.
Makarewicz, J.C., Likens, G.E., 1975. Niche analysis of a zooplankton community. Science 190, 1000–1003.
McCune, B., 2006. Non-parametric habitat models with automatic interactions. J. Veg. Sci. 17, 819–830.
Qian, S.S., King, R.S., Richardson, C.J., 2003. Two methods for the detection of environmental thresholds. Ecol. Mod. 166, 87–97.
Raffa, K.F., Aukema, B.H., Bentz, B.J., Carroll, A.L., Hicke, J.A., Turner, M.G., Romme, W.H., 2008. Cross-scale drivers of natural disturbances prone to anthropogenic amplification: the dynamics of bark beetle eruptions. BioScience 58, 501–517.
Raffa, K.F., Aukema, B.H., Erbilgin, N., Klepzig, K.D., Wallin, K.F., 2005. Interactions among conifer terpenoids and bark beetles across multiple levels of scale: an attempt to understand links between population patterns and physiological processes. Rec. Adv. Phytochem. 39, 80–118.
Scheffer, M., Carpenter, S.R., 2003. Catastrophic regime shifts in ecosystems: linking theory to observation. Trends Ecol. Evol. 18, 648–656.
Scheffer, M., Hosper, S.H., Meijer, M.L., Moss, B., Jeppesen, E., 1993. Alternative equilibria in shallow lakes. Trends Ecol. Evol. 8, 275–279.
Sperry, J.S., Donnelly, J.R., Tyree, M.T., 1988. A method for measuring hydraulic conductivity and embolism in xylem. Plant Cell Environ. 11, 35–40.
Thom, R., 1989. Structural Stability and Morphogenesis: An Outline of a General Theory of Models. Addison-Wesley, Massachusetts, p. 348.
Toms, J.D., Lesperance, M.L., 2003. Piecewise regression: a tool for identifying ecological thresholds. Ecology 84, 2034–2041.
U.S. Climate Change Science Program and the Subcommittee on Global Change Research, 2009. Thresholds of Climate Change in Ecosystems. USCCP Publication, Virginia, USA.
Vogt, U.K., 2001. Hydraulic vulnerability, vessel refilling, and seasonal courses of stem water potential of Sorbus aucuparia L. and Sambucus nigra L. J. Exp. Bot. 52, 1527–1536.
Waring, R.H., Major, J., 1964. Some vegetation of the California coastal redwood region in relation to gradients of moisture, nutrients, light, and temperature. Ecol. Monogr. 34, 167–215.
Weng, G., Bhalla, U.S., Iyengar, R., 1999. Complexity in biological signaling systems. Science 284, 92–96.
Whittaker, R.H., 1975. Communities and Ecosystems, second ed. Macmillan, New York, p. 385.
Womble, W.H., 1951. Differential systematics. Science 114, 315–322.